

A Co-Planar Waveguide Ultra-Wideband Antenna for Ambient Wi-Fi RF Power Transmission and Energy Harvesting Applications

Nuraiza Ismail^{1,*}, Ermeey Abd Kadir²

¹School of Electrical Engineering, College of Engineering, Universiti Teknologi MARA, Shah Alam, Malaysia

²School of Electrical Engineering, College of Engineering, Universiti Teknologi MARA, Terengganu, Malaysia

Received 25 January 2023; received in revised form 13 May 2023; accepted 14 May 2023

DOI: <https://doi.org/10.46604/ijeti.2023.11444>

Abstract

This study proposes an ultra-wideband antenna for ambient radio frequency (RF) energy harvesting applications. The antenna is based on a co-planar waveguide (CPW) transmission line and incorporates a rectangular slot as an antenna harvester. The proposed antenna utilizes an evolutionary design process to achieve impedance matching of the 50 Ω CPW feeding line over the desired frequency bands. A parametric study investigates CPW elements and rectangular slot size. The harvester antenna is then connected to the primary rectifier circuit of the voltage doubler to examine the signal characteristics. The antenna covers the Industry, Science, and Medicine (ISM) Wi-Fi bands of 2.45 GHz and 5 GHz, achieving a realized gain of 3.641 dBi and 4.644 dBi at 2.45 GHz and 5 GHz, respectively. It exhibits a relatively broad frequency ranging from 2.16 GHz to 6.32 GHz, covering the ultra-wideband fractional bandwidth (FBW) of 105%.

Keywords: rectangular slot antenna, co-planar waveguide (CPW), ultra-wideband (UWB) antenna, voltage doubler circuit, RF energy harvesting

1. Introduction

Microstrip antennas are widely used in wireless communication systems due to their compact size, low profile, ease of integration with printed circuit boards, and capability to integrate with monolithic microwave integrated circuits [1-2]. In recent years, there has been growing interest in using microstrip antennas for radio frequency (RF) energy harvesting applications, particularly for ultra-wideband (UWB) systems. Co-planar waveguide (CPW) antennas are another type of planar antenna that can be used for RF energy harvesting applications. CPW antennas have several advantages over other antennas, including a simple design and a low profile. CPW antennas are designed using a metal strip that is placed on a dielectric substrate, with a ground plane on the other side of the substrate. The metal strip and ground plane are separated by a gap, which is typically 50 ohms in impedance. The CPW antenna's planar structure and coplanar waveguide transmission line make it well-suited for energy harvesting applications, as it can be easily integrated into a PCB and has a wide bandwidth that can capture a range of RF signals.

Over the past decade, the use of the ambient environment as a source of RF energy harvesting has tremendously evolved for energizing low-power wireless electronic devices. These devices are commonly found in wireless sensor networks of the Internet of things (IoT), wearable electronic devices, and implantable biomedical devices [3-6]. As ambient RF energy harvesting results in an environmentally friendly and autonomous operation, this alternative solution offers cost savings by obviating the need for battery replacements and reducing regular energy-related maintenance downtime [5, 7]. The technology

* Corresponding author. E-mail address: nurais360@uitm.edu.my

requires a rectifying antenna in the receiving part, which consists of an antenna that captures the incident RF energy and performs as a transducer between propagating and guided waves. The RF energy is then rectified, converted to low-power DC voltage by a rectifier, and stored for future use [8-9].

The antenna for RF energy harvesting must possess a broad operating frequency range and the potential to radiate evenly in all directions. The incoming RF signal is from ambient electromagnetic waves, often with random polarization and arbitrary incidence angles. In light of this, the antenna design should have an omnidirectional radiation pattern. Numerous antenna designs have been published as antenna harvesters for RF energy harvesting applications capable of thriving in single-band, dual-band, multiband, and UWB [10]. Designing a single-band or multiband antenna that covers the whole band while maintaining high performance is difficult [11]. The designed UWB antenna is a promising solution to cover broad frequency ranges and maximize harvested power in wireless communication systems [12].

The United States Federal Communications Commission (FCC) has released an amendment (Part 15) that specifies the regulations governing the transmission and reception of UWB signals, allowing the signal power to spread over a large bandwidth range from 3.1 GHz to 10.6 GHz. According to this approval, a UWB signal is defined as any signal with a fractional bandwidth (FBW) equal to or larger than 0.20 of the center frequency or a bandwidth equal to or greater than 500 MHz [13]. The equations of the FBW, f_B , and the center frequency, f_c , can be obtained by:

$$f_B = \frac{2(f_H - f_L)}{f_H + f_L} \quad (1)$$

$$f_c = \frac{f_H + f_L}{2} \quad (2)$$

where f_H is the upper boundary and f_L is the lower boundary frequency.

This work proposes an antenna harvester based on a rectangular slot patch antenna with a CPW feed line using a low-cost flame retardant type 4 (FR-4) substrate. The design of the antenna harvester aims to capture RF ambient input signals in the Industry, Science, and Medicine (ISM) Wi-Fi bands of 2.45 GHz and 5 GHz resonant frequencies for RF energy harvesting applications. Since ambient EM waves typically have arbitrary polarization and random incident angles, the antenna for RF energy harvesting should have an omnidirectional radiation pattern and a wide operational frequency band. As a result, it is intended to design a harvester antenna that can operate over a broad ambient signal spectrum, referred to as UWB, covering frequency bands ranging from 2 GHz to 6 GHz with an omnidirectional radiation pattern. The proposed frequency bands work under FCC regulations under the surveillance systems frequency bands of 1.9 GHz to 10.6 GHz [14] and within the 2.17 GHz to 10.6 GHz radar imaging operating frequency band, which is under the Malaysian Communications and Multimedia Commission (MCMC) [15].

2. Antenna Design Configuration

The design of a receiving antenna involves the selection of an antenna substrate, antenna patch shape, and determination of the waveguide feedline. Fig. 1 illustrates the top-view antenna arrangement with the design parameters covering the 2.45 GHz and 5 GHz Wi-Fi frequency bands based on the CPW feedline. The signal is typically fed into a 50 Ω CPW via a Sub-Miniature version A (SMA) connection. It comprises a rectangular patch and a rectangular slot in the middle of the patch. The antenna feedline is designed based on a CPW, and the type of substrate used is FR-4.

The FR-4 substrate is chosen because it is widely available, simple to fabricate, and relatively inexpensive compared to other high-performance substrate materials like Rogers [16]. While Rogers substrates generally offer better electrical performance than FR-4, their cost, and availability can be limiting factors for some applications. In RF energy harvesting

applications where cost-effectiveness and mass production are essential, using FR-4 can provide a good balance between performance and cost. Furthermore, FR-4 can provide adequate performance for many RF energy harvesting applications, particularly those operating at lower frequencies.

The cross-sectional view of the CPW, as depicted in Fig. 2, is a uniplanar transmission line with the ground on the same surface as the feedline with the CPW on each side. The copper portion is shown in light blue and golden, while the white substrate is shown in white. This configuration is favored for this work due to its simple impedance matching and the high circuit density on a single layer. In conjunction with this, its active and passive elements are easy to integrate and endure with minimal dispersion and radiation loss [17]. All these features make the CPW an appropriate solution for rectifying designs.

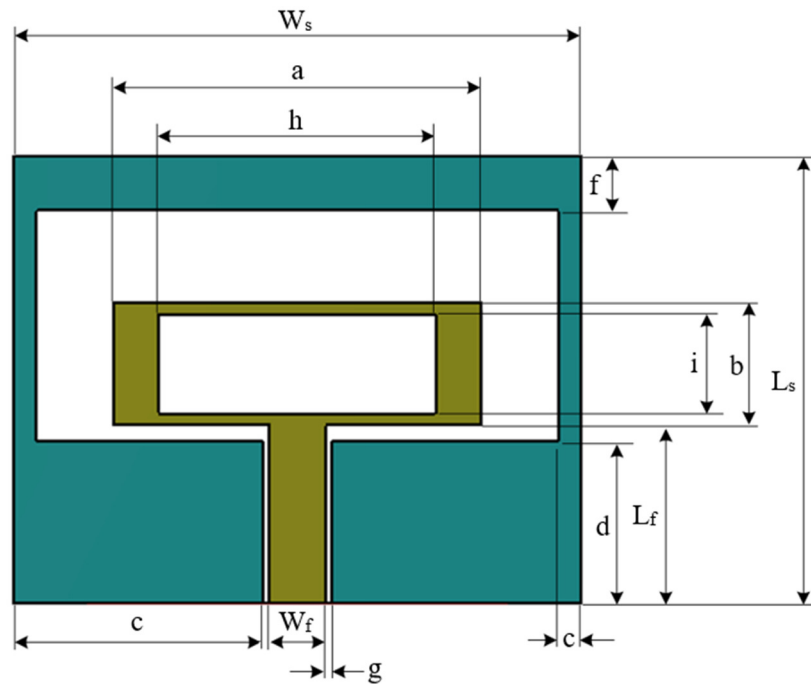


Fig. 1 Geometry of the developed UWB antenna harvester

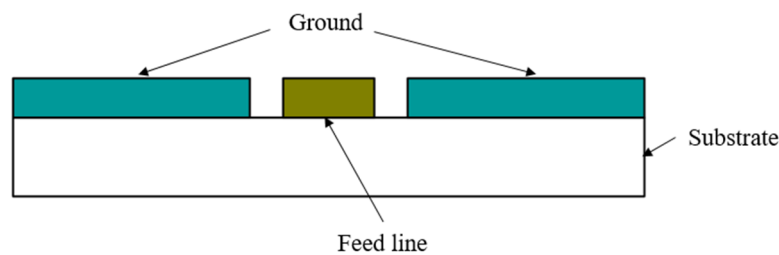


Fig. 2 Cross-sectional view of the feed line of the developed antenna harvester

The low-cost printed circuit board FR-4 substrate with a dielectric constant of 4.7, a loss tangent of 0.025, and a thickness of 1.6 mm is used for designing the proposed CPW antenna. The width and length are calculated using

$$W = \frac{c}{2f_r} \sqrt{\frac{2}{\epsilon_r + 1}} \tag{3}$$

$$L = \frac{c}{2f_r \sqrt{\epsilon_r}} \tag{4}$$

where the velocity of light in free space is denoted by c , which equals $3 \times 10^8 \text{ ms}^{-1}$, the resonant frequency is denoted by f_r , and the dielectric constant of the substrate is denoted by ϵ_r .

After the dimensions of the patch had been figured out, the design of the feeding line for the rectangular patch antenna was created. It is essential to design this feeding line to enable signal transmission from an SMA connector to the radiating element of a patch antenna. The currently offered SMA connectors come with various characteristic impedance values. For this research, the antenna excited by an SMA with a 50Ω characteristic impedance was selected. Therefore, the designed feeding line should also have a characteristic impedance of 50Ω to achieve impedance matching. The following is an equation utilized to obtain the width of the feeding line.

$$Z_{feed} = \frac{87}{\sqrt{\epsilon_r + 1.41}} \ln \left(\frac{5.98h}{0.8W_{feed}} \right) \quad (5)$$

The characteristic impedance of the feeding line is given by Z_{feed} . The thickness of the substrate is denoted by h , while W_{feed} is the width of the feeding line.

After optimization, the detailed geometric structure of the proposed antenna design is listed in Table 1, where the antenna is excited by a feeding line of 50Ω characteristic impedance with a width of 3.662 mm. The gaps between the feeding line and the right and left sides of CPW are denoted by g , which is equal to 0.4 mm.

Table 1 The Optimization parameters of the developed antenna harvester

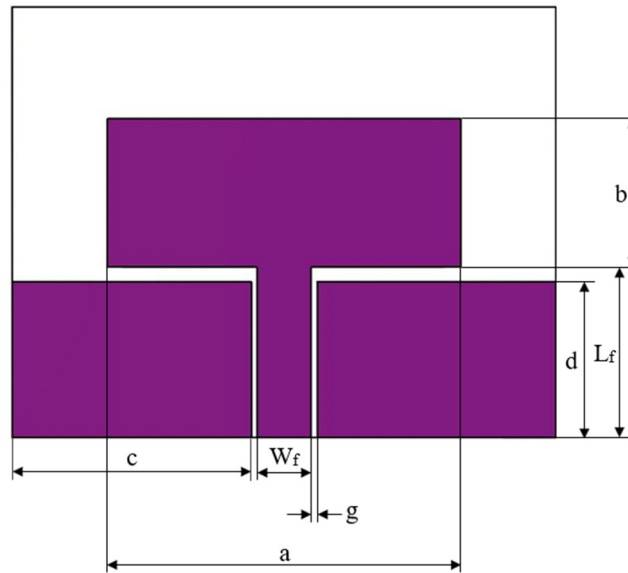
Parameters	Descriptions	Dimension (mm)
a	Width of rectangular patch	24
b	Length of rectangular patch	8
c	Width of CPW	16.269
d	Length of CPW	10.5
e	Width of side ground plane	1.5
f	Length of the top ground plane	4
g	The gap between the feedline and CPW	0.4
h	Width of the inner rectangular slot	18
i	Length of the inner rectangular slot	12
W_s	Width of substrate	37
L_s	Length of substrate	29
W_f	Width of feedline	3.662
L_f	Length of feedline	11.5

3. Parametric Study

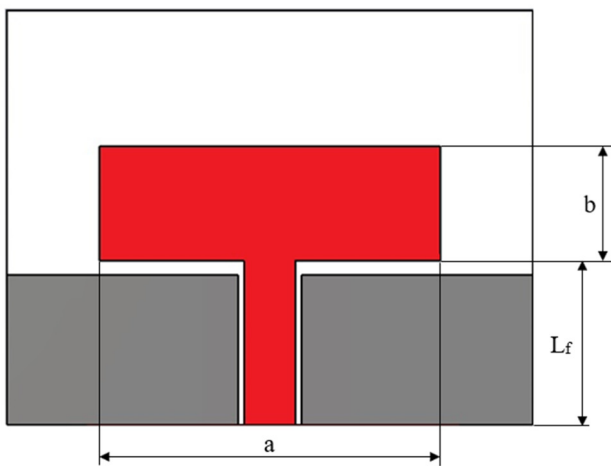
The design of the proposed antenna harvester covering two Wi-Fi frequency bands involves many geometrical parameters, as depicted in Fig. 1. A parametric study was performed to achieve a satisfactory frequency response of the reflection coefficient, which is less than -10 dB while maintaining 50Ω impedance matching throughout the desired frequency bands. For this work, the antenna aims to operate omnidirectionally, which can radiate in the same pattern to all 360 degrees of direction. Therefore, the effects of parameters on the antenna's performance were investigated stage by stage using CST Microwave studio software in terms of line impedance matching, return loss, and radiation pattern. Two significant parameter elements were configured: the CPW element and the rectangular slot size. The development of a harvester antenna with an evolutionary design structure is illustrated in Fig. 3.

The first step in developing the proposed antenna is to design the preliminary antenna structure, as depicted in Fig. 3(a). The patch antenna is designed using the values of the parameters shown in Table 2, where the width, length, and line impedance width of the patch are calculated using Eqs. (3), (4), and (5), respectively. A comparative parametric study will be conducted to analyze the effect of various modifications on the rectangular patch antenna's performance. These modifications include altering the antenna size and feedline length, adjusting CPW-element 1 and CPW-element 2, as well as adding a rectangular

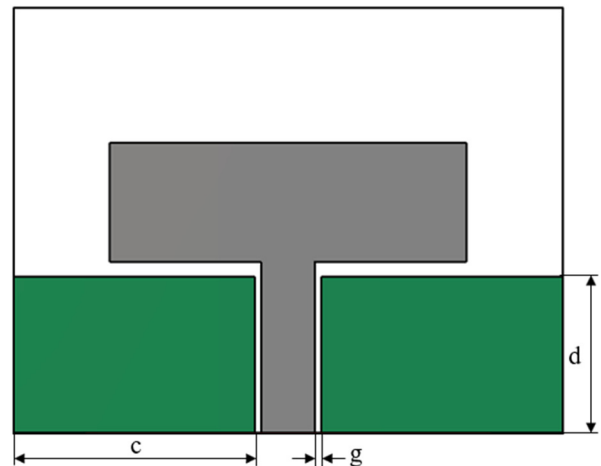
slot as shown in Fig. 3(b), (c), (d), and (e), respectively. The analysis will focus on evaluating their effects on line impedance matching and return loss. The antenna structure will be integrated with the voltage doubler circuit if the return loss and line impedance are less than 10 dB and approximately 50 Ω, respectively. The connection between the antenna and circuit performance will be examined in terms of S-parameters for the magnitude of return loss, $|S_{11}|$ and transfer coefficient, $|S_{21}|$. The results of parametric studies are discussed in the following subsection.



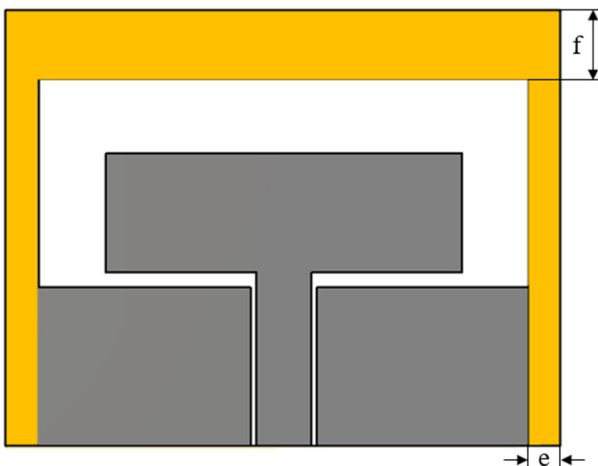
(a) Preliminary antenna design



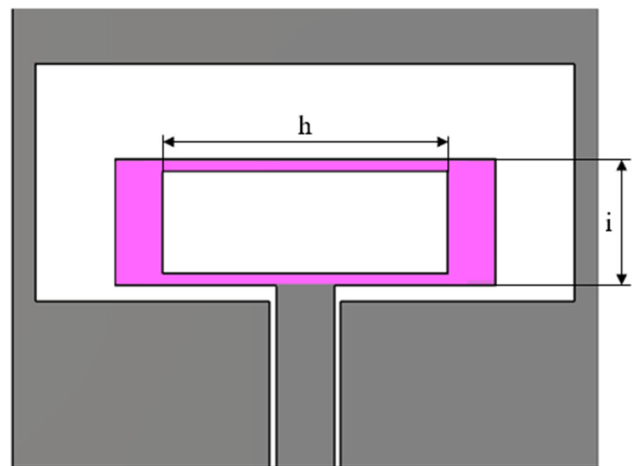
(b) Patch antenna



(c) CPW-element 1



(d) CPW-element 2



(e) Rectangular slot

Fig. 3 Antenna evolutionary design structure

Table 2 The preliminary parameters values of the proposed harvester antenna

Parameters	Dimensions (mm)
a	22.48
b	17.05
c	17.169
d	17.98
g	0.5
l	37
m	40
W_f	3.662
L_f	18.98

4. Design Analysis

The analysis of the proposed antenna harvester of the evolutionary design has started with the preliminary antenna design structure. Then the effects of the rectangular patch antenna and feedline length were analyzed. After that, an analysis was performed to determine how the CPW size of elements 1 and 2 and a rectangular slot affected the antenna's reflection coefficient. Further analysis was carried out to analyze the harvester antenna's performance when connected to the rectifier circuit.

4.1. Preliminary antenna design

The antenna structure shown in Fig. 3(a) indicates the initial design parameters that influence the antenna impedance characteristic. These parameters are denoted as a, b, c, d, g, W_f , and L_f . Fig. 4 illustrates the simulated reflection coefficient, S_{11} result for the preliminary parameter values listed in Table 2. The antenna bandwidth is typically measured at -10 dB as it represents the point where the signal's power level received or transmitted by the antenna decreases to 10% of its maximum value. This is known as the "half-power point" or the "3 dB point," which represents the frequency point where the antenna's gain is reduced by 3 dB from its maximum value. As observed, the S_{11} remains above -10 dB. The antenna line characteristic impedance is mismatched at 50 Ω , as depicted in Fig. 5.

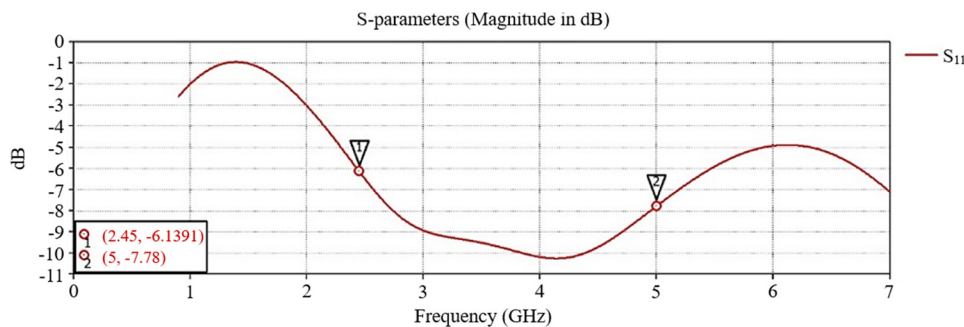


Fig. 4 Simulated S_{11} for the preliminary antenna design structure

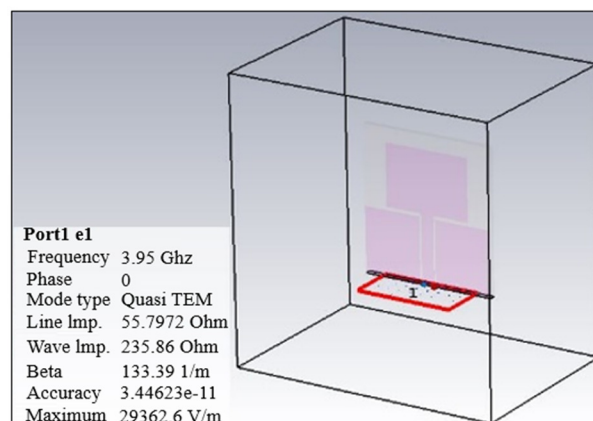


Fig. 5 Line impedance of preliminary antenna design structure

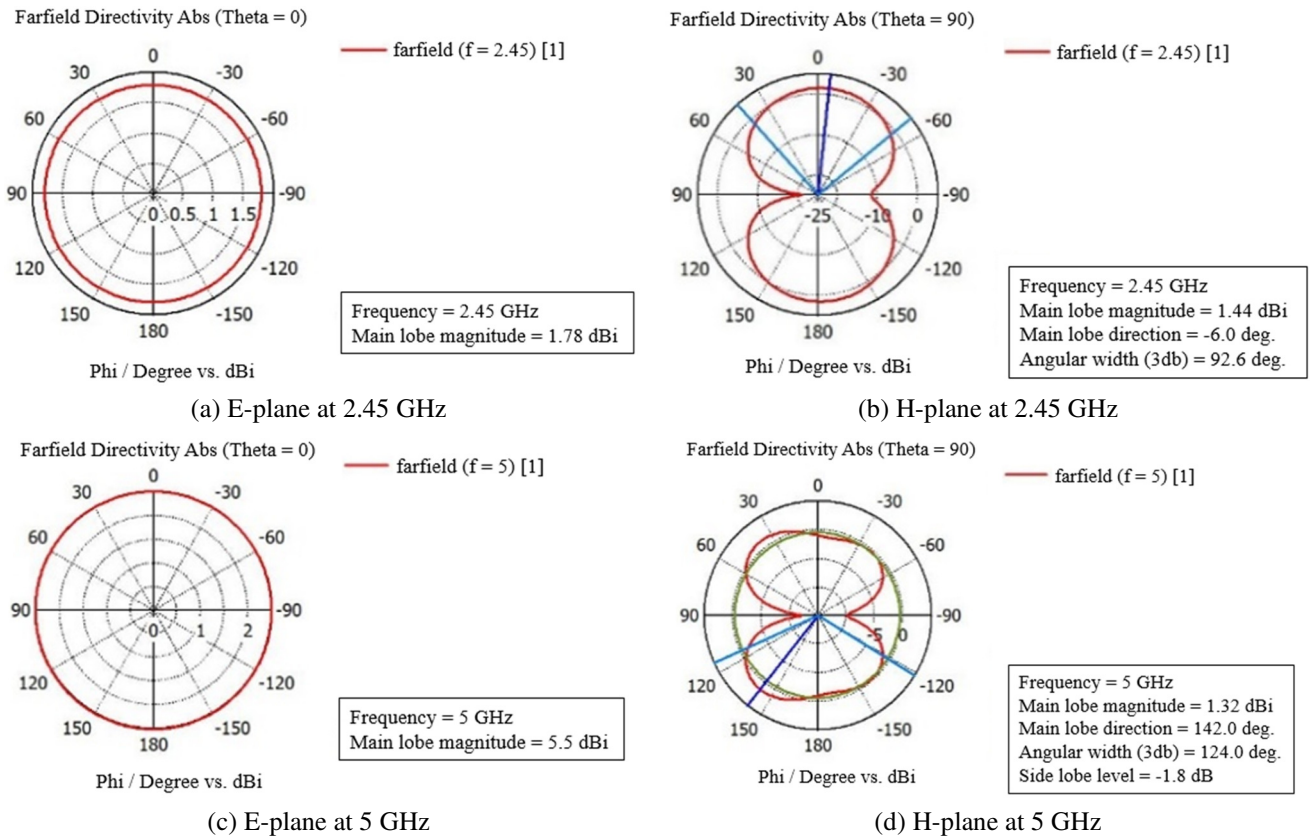


Fig. 6 Polar plot radiation pattern of the preliminary antenna

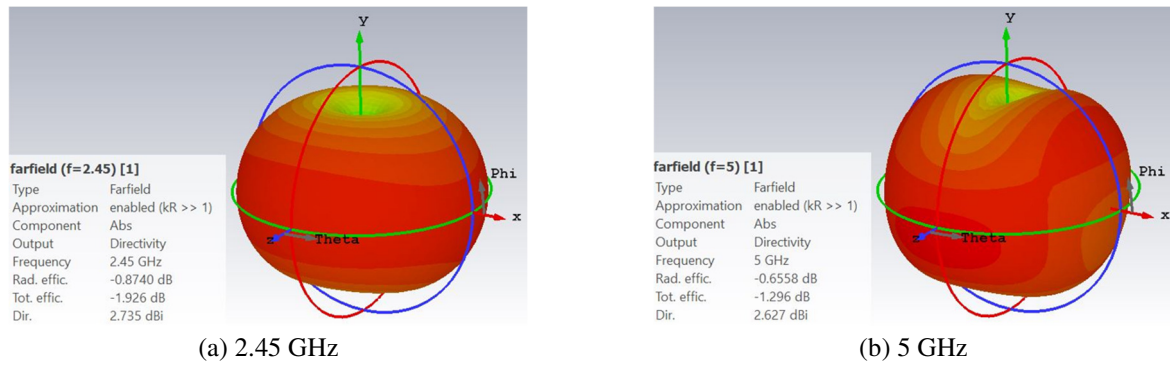


Fig. 7 3D antenna radiation pattern

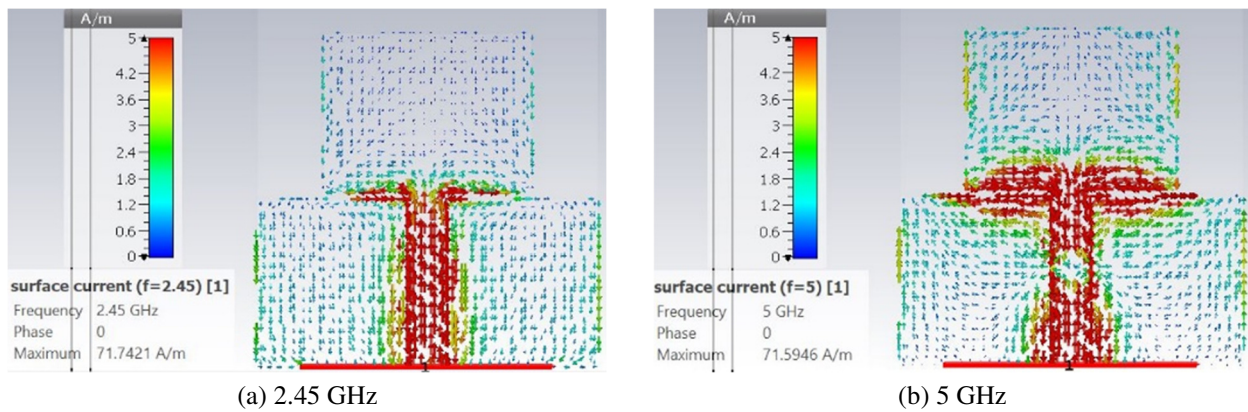


Fig. 8 The surface current distribution of the preliminary antenna design

The simulation antenna polar plot radiation pattern at resonant frequencies of 2.45 GHz and 5 GHz in the E-plane (z-y plane) and the H-plane (x-z plane) is presented in Fig. 6. The antenna radiates perfectly omnidirectionally in the E-plane at both frequencies. In contrast, the antenna generates symmetrical patterns in the H-plane and exhibits nulls at theta values of -

90° and 90°. Fig. 7 depicts the preliminary antenna gains of 2.735 dBi and 2.627 dBi at 2.45 GHz and 5 GHz, respectively. The surface current distribution at both frequencies is shown in Fig. 8. Most of the surface currents are primarily distributed along the feedline, as evident. On the other hand, minority surface currents are dispersed throughout both the CPW and patch antenna.

4.2. Effect of the rectangular patch antenna and feedline length

The effect of the rectangular patch antenna and feedline length were examined by modifying the sizes of a, b, and L_f . In this second stage, the antenna performance is focused on achieving a 50 Ω matching impedance and comparing the reflection coefficient, rather than evaluating the radiation pattern and antenna gain. The preliminary antenna led to a mismatched condition.

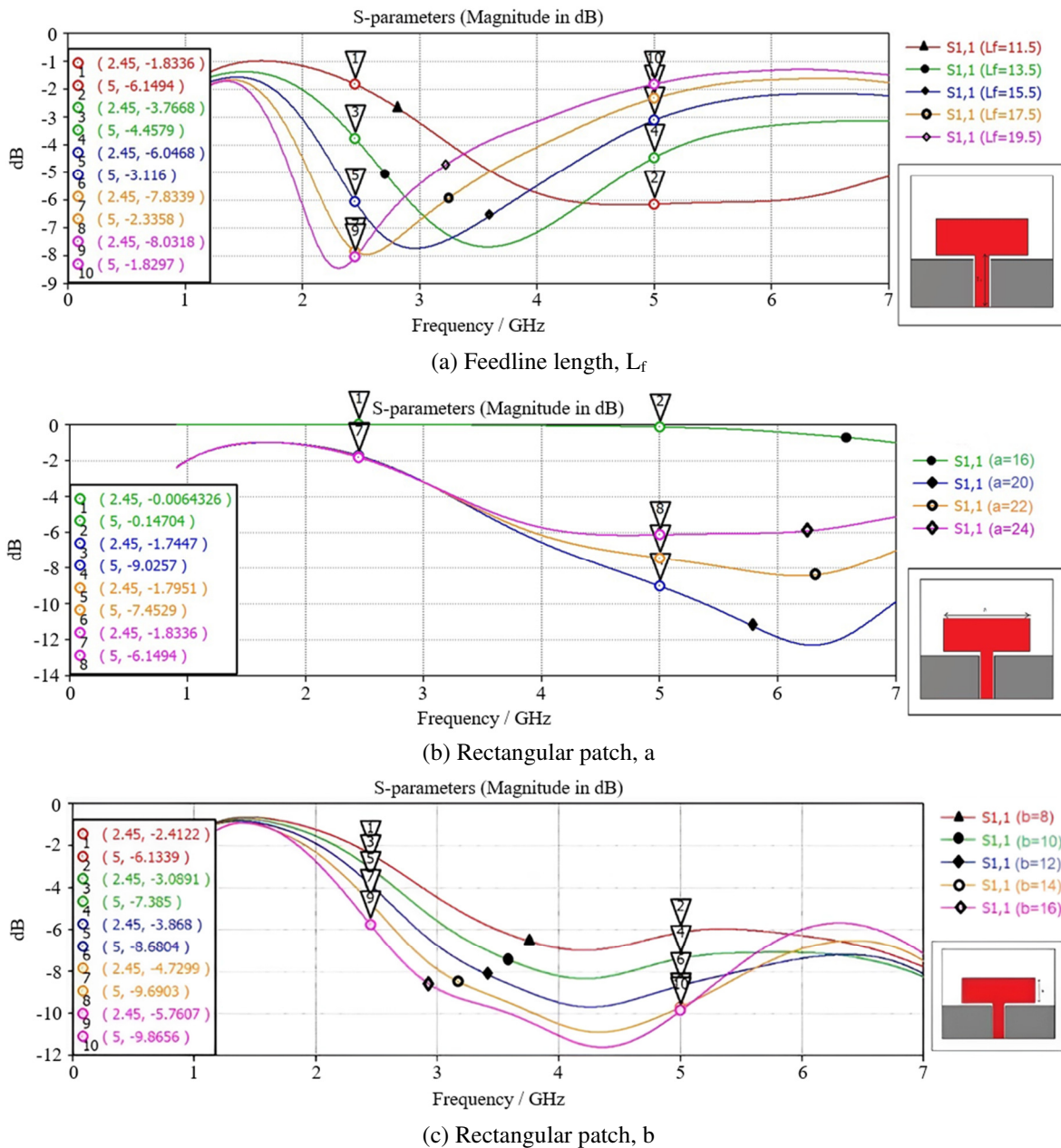


Fig. 9 The effect of varying the rectangular patch antenna and feedline length

The optimization was performed on the rectangular patch while maintaining the feedline width, W_f , and the gap between the feedline and the CPW, g. The length of CPW, d, was tuned based on the change in feedline length, L_f , and t. To prevent overlap between d and L_f , the gap between them was maintained at the same value of 1 mm, as specified in the preliminary

parameters. Fig. 9 and Fig. 10 depict the magnitude of S_{11} and the line impedance while varying the parameters L_f , a , and b , respectively. The feedline length, patch length, and width were varied by as much as 2 mm, 4 mm, and 2 mm for every step, respectively. The antenna exhibits an impedance mismatch at the desired frequencies of 2.45 GHz and 5 GHz for all the varying parameters. Furthermore, the transmission line impedance is similar to that of the preliminary antenna, which is much greater than 50 Ω .

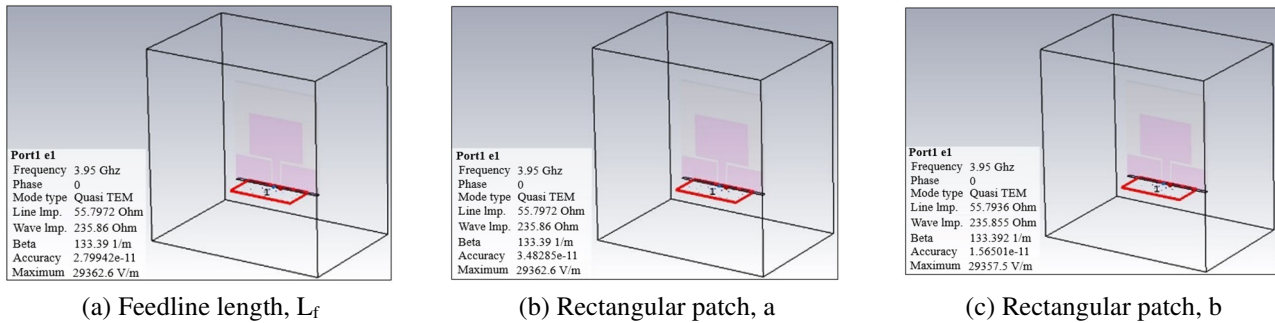


Fig. 10 Line impedance of varying the rectangular patch antenna and feedline length

Since the variation of the rectangular patch antenna and feedline length did not satisfy the antenna performance, the effect of modifying the CPW for element 1 is investigated in the following subsection. The parameter values of $L_f = 11.5$ mm, $a = 24$ mm, and $b = 8$ mm are selected in the next evolutionary design of the antenna. $L_f = 11.5$ mm and $a = 24$ mm are selected as both apparent UWB compared to other parameter values, as shown in Fig. 9(a) and (b), respectively. Furthermore, the parameter $b = 8$ mm is preferred because it reduces the antenna size, as shown in Fig. 9(c). Thus, the length of the substrate has also been reduced as the length of the rectangular patch is reduced.

4.3. Effect of CPW size – element 1

The second stage in the parametric analysis is to investigate the effect of varying the size of the CPW, as shown in the green element in Fig. 3(c). The optimization of CPW length, c , was optimized by varying the gap between the feedline and the CPW, denoted by g . Fig. 11 illustrates the effect on the reflection coefficient, S_{11} , when the gap, g , was varied from 0.3 mm to 0.7 mm in steps of 1 mm. None of the gap variations influence the antenna’s performance in terms of return loss, as evident. On the other hand, adjusting the gap, g has affected the antenna transmission line impedance, as depicted in Fig. 12. As a result, the optimal parameter value, g is equal to 0.4 mm, is selected since it is relatively close to 50 Ω .

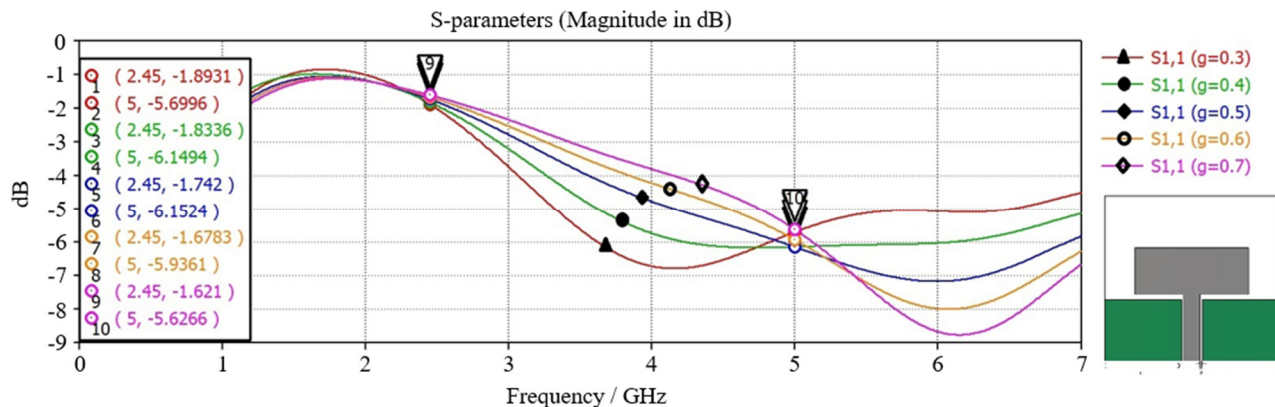


Fig. 11 The effect on the reflection coefficient, S_{11}

The parametric study continued to find out how the size of the CPW affects the antenna’s performance. The length of CPW, d was tuned from 8.5 mm to 10.5 mm using five samples while utilizing the optimized CPW width, c , with a set gap of 0.4. Fig. 13 shows how varying the CPW length affects the reflection coefficient. Once again, it is observed that no variation for the parameter could reach $S_{11} < -10$ dB. As a result, this leads to the conclusion that an impedance mismatch occurred over

the entire CPW size for element 1. Nevertheless, when the gap, g , is 0.4 mm, the transmission line impedance can be achieved at approximately 50Ω . The CPW length, d is equal to 10.5 mm and has been selected for the following antenna evolutionary design as it is perceived as UWB compared to other parameter values.

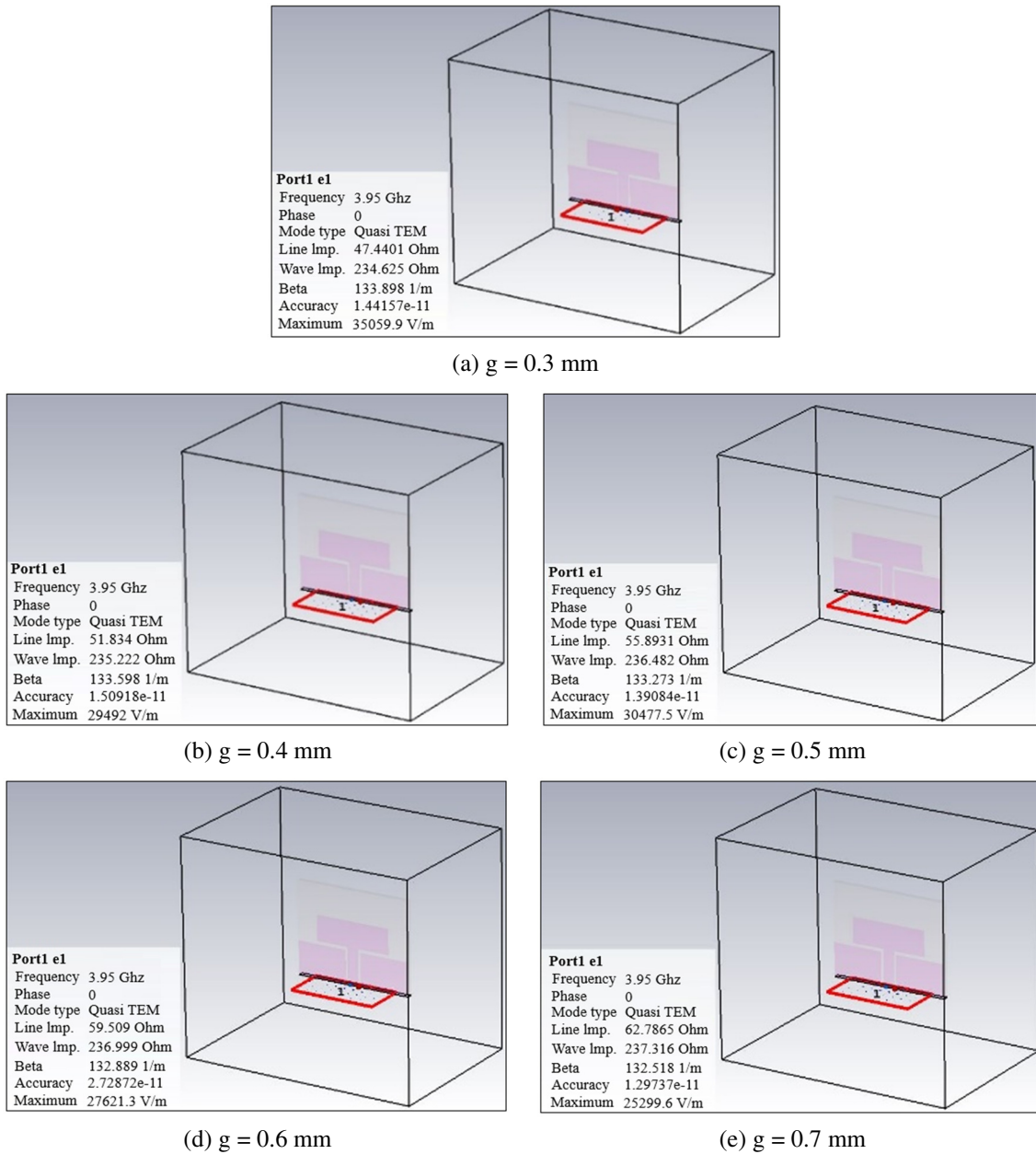


Fig. 12 The effect on the line characteristic impedance

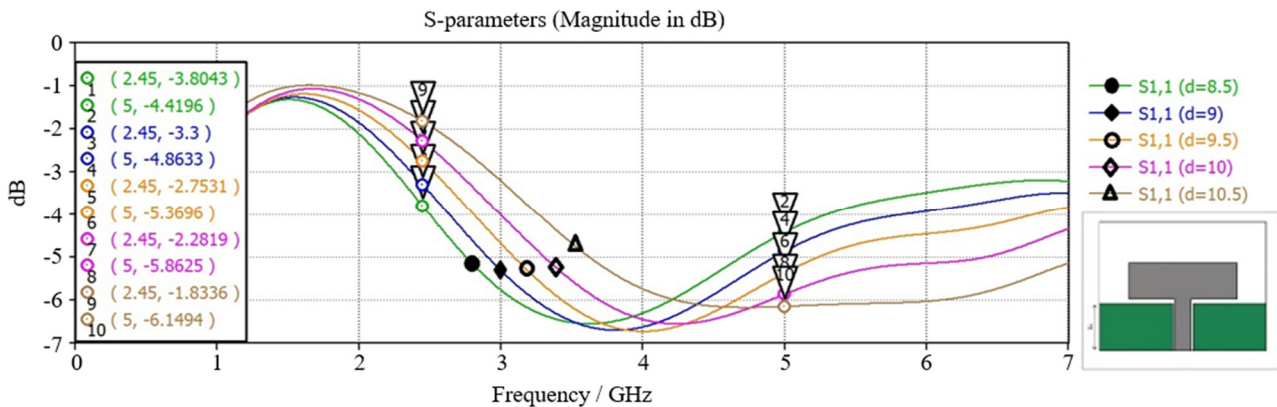


Fig. 13 The effect of varying the length of CPW, d

4.4. Effect of CPW size – element 2

Next, the evolutionary antenna design was further investigated based on the CPW size of element 2. This investigation involved varying the width and length of the side and top of the ground plane, denoted by e and f , respectively, as illustrated in Fig. 3(d). The investigation is focused on achieving matching impedance to attain a reflection coefficient of more than 10 dB. This goal arises from the previous evolutionary stage, where the transmission line characteristic impedance was satisfied at approximately 50Ω . Fig. 14 demonstrates that by varying the width of the side CPW(e) from 1 mm to 3 mm in increments of 0.5 mm, only three parameter sizes resulted in achieving S_{11} values less than -10 dB at 2.45 GHz frequency. At 5 GHz, however, all parameters exhibited an impedance mismatch.

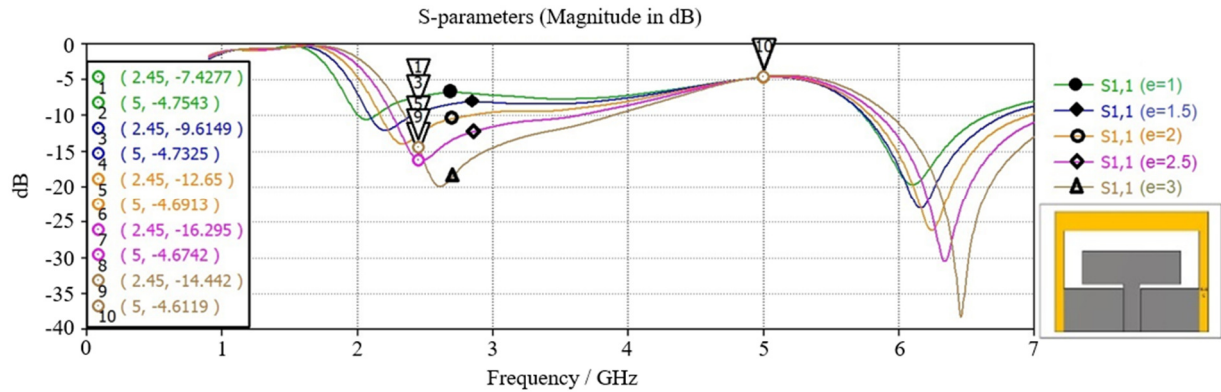


Fig. 14 The effect of varying the width of the side ground plane, e

Even though the variation of CPW width did not satisfy impedance matching for both 2.45 GHz and 5 GHz frequencies, as e was set at 2 mm, 3 mm, and 3.5 mm, good impedance matching can be achieved over the 2.45 GHz band. Consequently, the length of the top ground plane, f , was varied for each set of variations in the width of the side ground plane ($e = 2$ mm, 3 mm, and 3.5 mm). Fig. 15 depicts the effect of varying the length of the top ground plane.

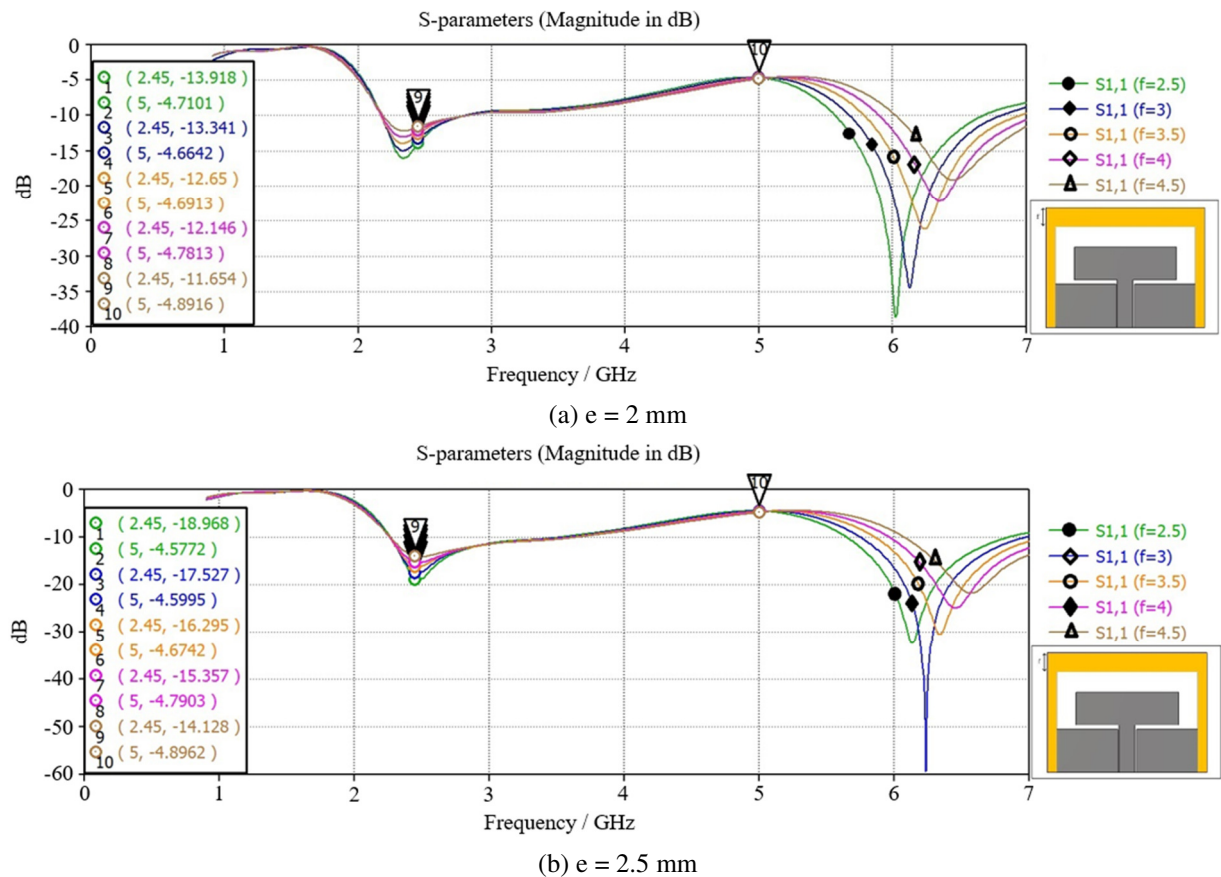


Fig. 15 The effect of varying the length of the top ground plane, f

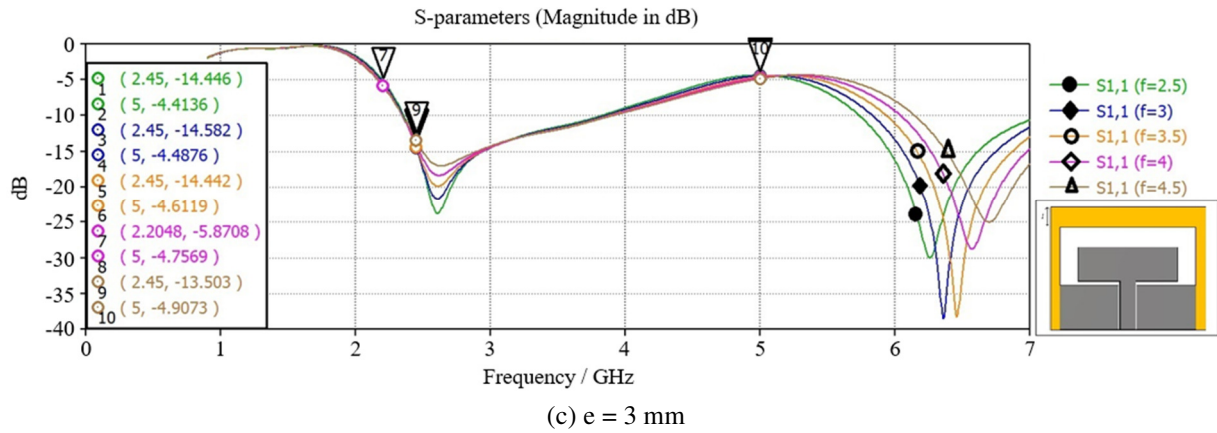


Fig. 15 The effect of varying the length of the top ground plane, f (continued)

As shown in Fig. 15(a) and (b), good impedance matching can only be achieved in the 2.45 GHz frequency band when the width, e , is set at 2 mm and 3 mm. Meanwhile, when e was set at 3.5 mm, an impedance mismatch at 2.45 GHz occurred only when the value of f was set to 4 mm. Additionally, none of the parameters achieved good matching at the 5 GHz frequency. Table 3 presents the effects of the optimization process. Comparing variations in the length of the top ground plane, f , and a set of the width of the side CPW, e , the most significant reflection coefficient is chosen when both parameters e and f are set as 2.5 mm.

Table 3 Detailed results of varying the length of the top ground plane, f

Parameters	Frequency (GHz)	Reflection coefficient, S_{11} (dB)				
		f = 2.5	f = 3.0	f = 3.5	f = 4.0	f = 4.5
e = 2.0	2.45	-13.9	-13.3	-12.7	-12.1	-11.7
	5	-4.7	-4.6	-4.6	-4.8	-4.8
e = 2.5	2.45	-18.9	-17.5	-16.3	-15.4	-14.1
	5	-4.6	-4.6	-4.7	-4.8	-4.9
e = 3.0	2.45	-14.4	-14.6	-14.4	-5.8	-13.5
	5	-4.4	-4.9	-4.6	-4.8	-4.9

4.5. Effect of a rectangular slot

The parametric investigation has been carried out on the rectangular slot size since the matching impedance has only been accomplished at 2.45 GHz so far. By adding the rectangular slot on the patch antenna, as illustrated in Fig. 3(e), the width, h , and length, i of the rectangular slot were varied to examine the antenna performance on the reflection coefficient for both 2.45 GHz and 5 GHz frequencies. The rectangular slot size was investigated in CST simulation software by simultaneously varying h from 15 mm to 19 mm in 1 mm increments and i from 4.5 mm to 6.5 mm in 0.5 mm steps. The frequency response of the reflection coefficient when varying the width, h , and length, i of the rectangular slot, as depicted in Fig. 16.

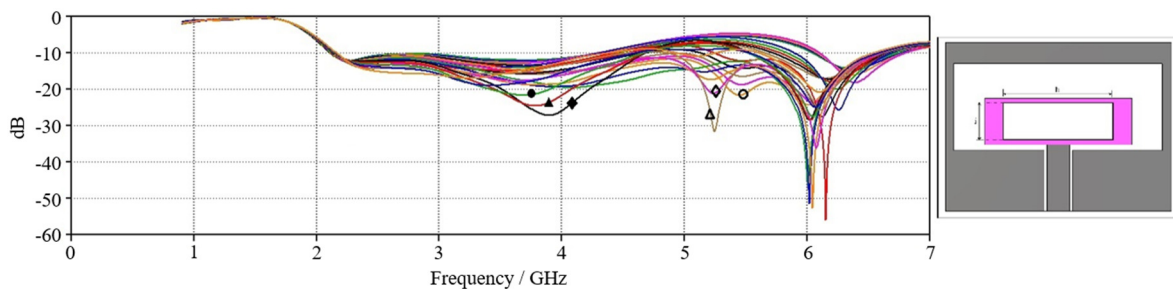


Fig. 16 The effect of varying the inner rectangular slot

Table 4 summarizes the reflection coefficient of the obtained simulations. As tabulated in Table 4, it can be observed that the parameter h equals 18 mm, has significant effects on the reflection coefficient while varying the rectangular slot width, i , and that matching impedance was achieved for both the 2.45 GHz and 5 GHz frequency bands. Since the parameter variation,

i exhibited decent results when h was set at 18 mm, choosing parameter i that provides the best results is necessary. As the reflection coefficients of -13.4 dB and 13.3 dB are similar for both frequency bands, the optimum value of i is chosen to be 6 mm in this study.

Table 4 Detailed reflection coefficient results of varying the width, h, and the length, i, of the rectangular slot

Parameters	Frequency (GHz)	Reflection Coefficient, S ₁₁ (dB)				
		i = 4.5	i = 5.0	i = 5.5	i = 6.0	i = 6.5
h = 15	2.45	-10.9	-11.1	-11.5	-11.9	-12.1
	5	-6.5	-6.3	-6.0	-5.7	-5.5
h = 16	2.45	-11.5	-11.4	-12.0	12.2	-12.9
	5	-8.0	-7.7	-7.4	-6.8	-6.1
h = 17	2.45	-11.6	-11.9	-12.4	-12.9	-13.7
	5	-11.8	-11.1	-10.3	-9.3	-8.0
h = 18	2.45	-12.0	-12.4	-12.9	-13.4	-14.4
	5	-14.6	-14.4	-14.0	-13.3	-12.0
h = 19	2.45	-12.2	-12.6	-13.2	-13.8	-14.9
	5	-6.8	-7.5	-8.2	-9.2	-10.6

Since the antenna design at this stage has achieved good matching impedance with parameters h and i set at 18 mm and 6 mm, respectively, other antenna performances are analyzed regarding VSWR, antenna directivity, radiation pattern, and surface current. It is noted that is efficient for both frequencies when the value of VSWR is less than or equal to 2, as depicted in Fig. 17.

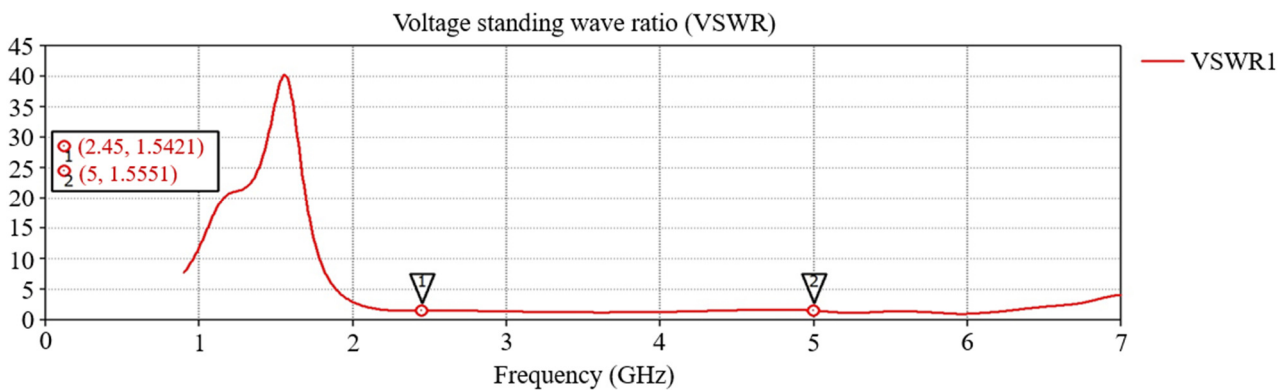


Fig. 17 Voltage standing wave ratio (VSWR) at 2.45 GHz and 5 GHz

Fig. 18 demonstrates the simulation antenna polar plot radiation pattern at resonant frequencies of 2.45 GHz and 5 GHz in the E-plane (z-y plane) and the H-plane (x-z plane). The antenna emits radiation in an omnidirectional pattern in the E-plane at both frequencies. However, the antenna forms symmetrical patterns in the H-plane, with nulls occurring at theta values of -90° and 90°.

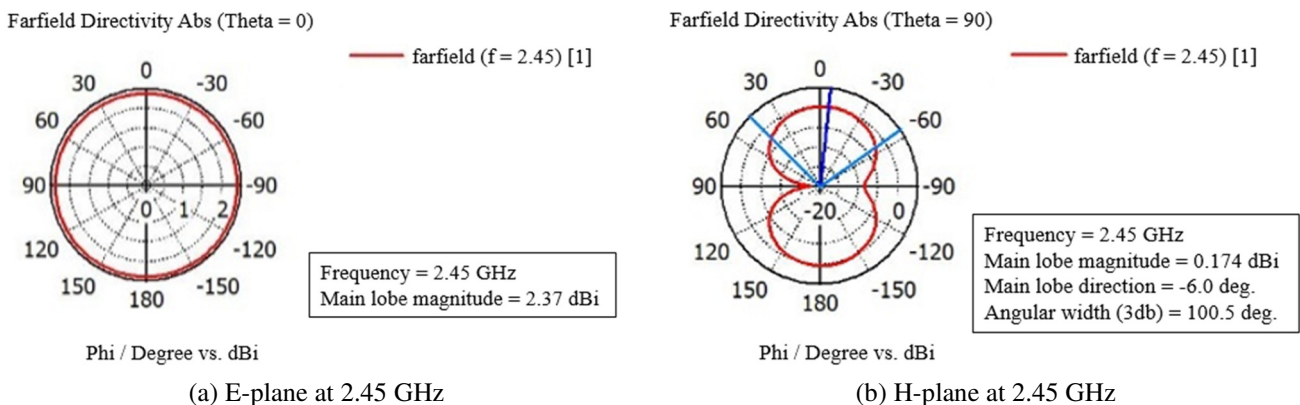


Fig. 18 Polar plot radiation pattern of adding a rectangular slot to a CPW

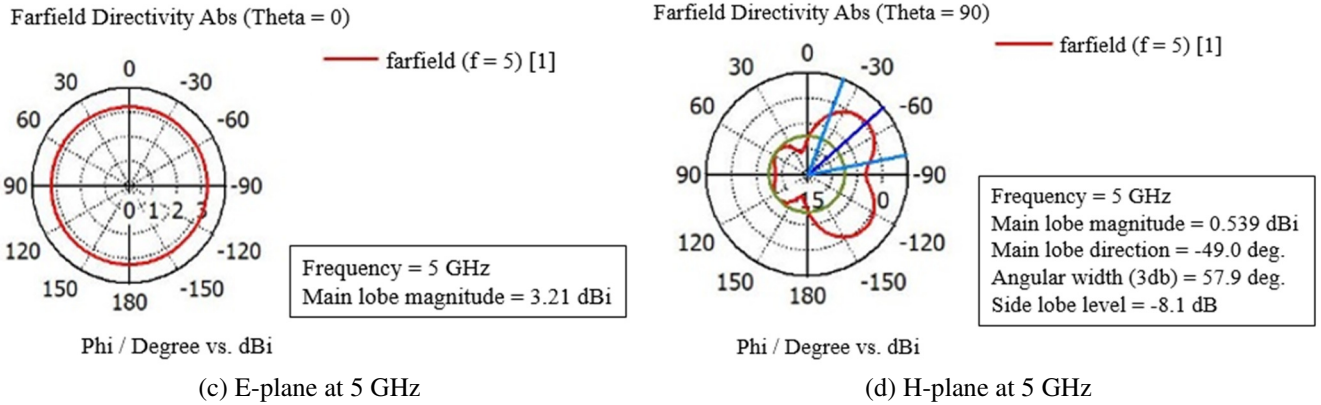


Fig. 18 Polar plot radiation pattern of adding a rectangular slot to a CPW (continued)

The gain at this evolutionary stage is demonstrated in Fig. 19. The result indicates that adding a rectangular slot to a CPW significantly increased the gain to 3.641 dBi and 4.644 dBi at 2.45 GHz and 5 GHz, respectively. Hence, it is found that the gain is an increment of 33% at 2.45 GHz and 77% at 5 GHz as compared to the preliminary antenna gains. Moreover, the maximum radiation efficiency of 72% and 68% is achieved at 2.45 GHz and 5 GHz, respectively. The distribution of the surface current at the frequencies of 2.45 GHz and 5 GHz when adding a rectangular slot with CPW is illustrated in Fig. 20. At 2.45 GHz, the majority of the surface currents are spread out along the feedline, the side of the CPW, and the top of it, as well as the bottom part of the antenna slot, as shown in Fig. 20(a). Meanwhile, when operating at a frequency of 5 GHz, most surface currents are dispersed along the feedline, the entirety of the rectangular slot, and some part of the CPW at the edge side.

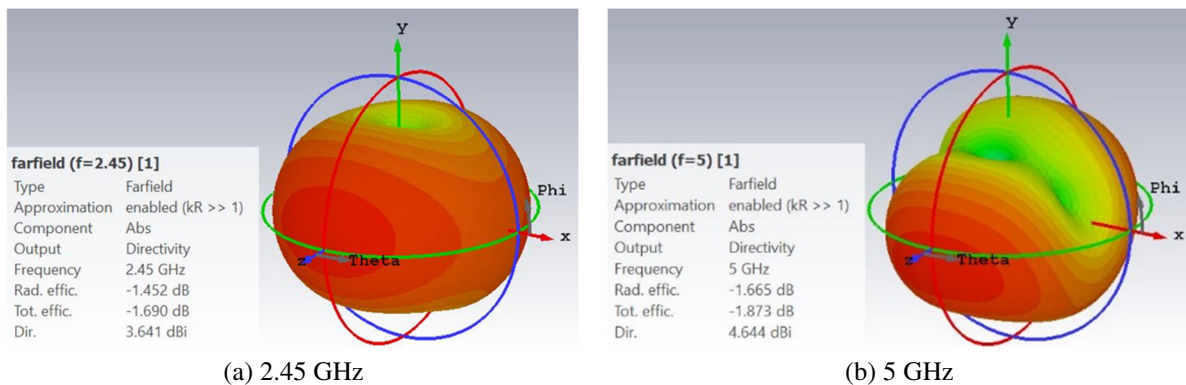


Fig. 19 3D antenna radiation pattern

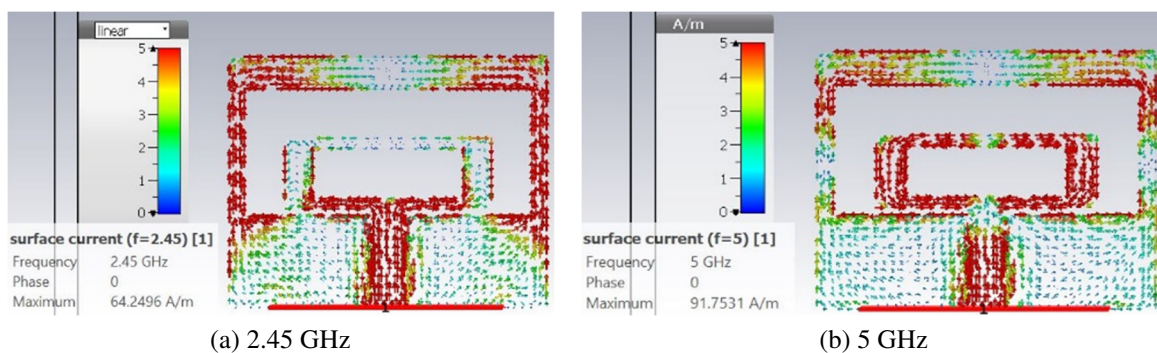


Fig. 20 The surface current distribution of the designed antenna

Although the antenna in this evolutionary stage has achieved good impedance matching in terms of reflection coefficient and satisfied the VSWR and other performance requirements, further investigation was carried out to determine how it performed when connected to the rectifier circuit. The antenna design, which consists of a CPW and rectangular slot, is connected to the rectifier circuit to scrutinize the signal characteristics of the harvesting system. As illustrated in Fig. 21, the

antenna design and rectifier circuit integration are carried out using CST Microwave Studio and integrated with CST Design Studio. The circuit topology is adopted based on a prominent rectifier voltage doubler, which revolves around two distinct components: the diode and the capacitor. The component value listed in Table 5 aligns with the approach proposed by Tafekirt et al. [18] and Sathiyapriya et al. [19]. Moreover, the prominent commercial Schottky diodes are compared between the SMS7630 and HSMS2852 series, as both are sufficient for the Wi-Fi frequency bands.

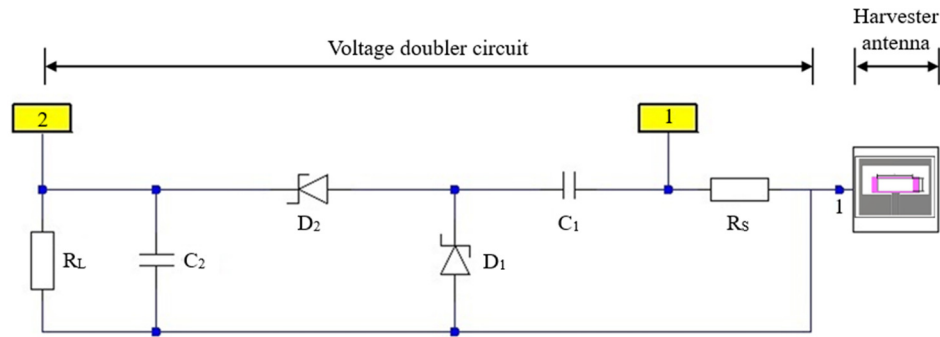
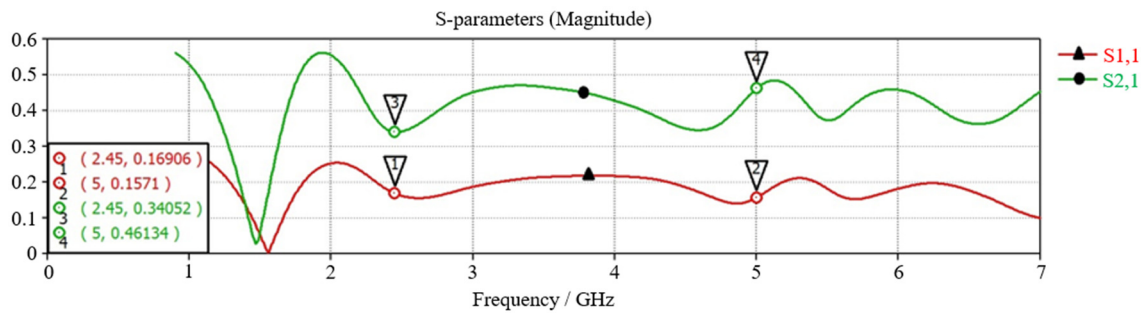


Fig. 21 The integration of the rectifier circuit with the proposed antenna harvester

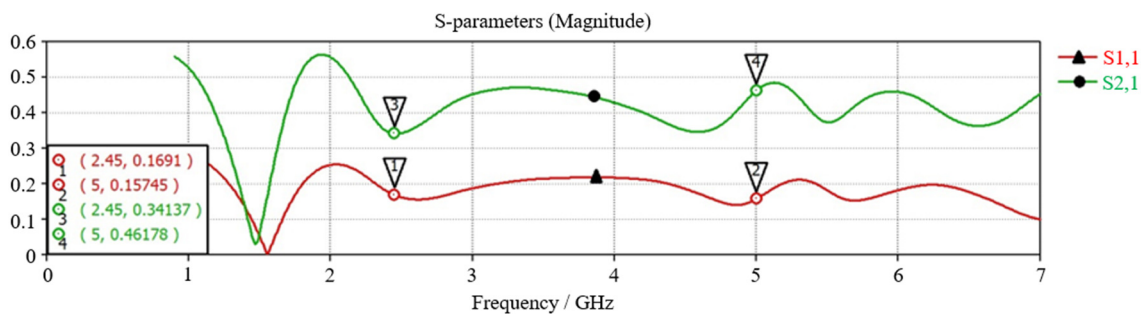
Table 5 Circuit components specifications

Parameters	Value
C_1 and C_2	47 μ F 100 pF
R_S	50 Ω
R_L	10 k Ω
D_1 and D_2	HSMS2852 SMS7630

The simulated results of the S-parameter in terms of reflection coefficient, S_{11} , and transfer coefficient, S_{21} of the designed antenna integrated with the voltage doubler circuit are represented in magnitude, as shown in Fig. 22. The S-parameter results might be expressed as either a magnitude or a decibel (dB) value. The value of the S_{11} parameter is intended to be close to or lower than 0.1, or when expressed in terms of dB, the value should be lower than -10 dB. Also, the value could be expressed in magnitude or dB for parameter S_{21} ; nevertheless, the parameter value needs to be relatively close to 1 or 0 dB.



(a) HSMS2852 and 47 μ F



(b) HSMS2852 and 100 pF

Fig. 22 The reflection and transfer coefficient

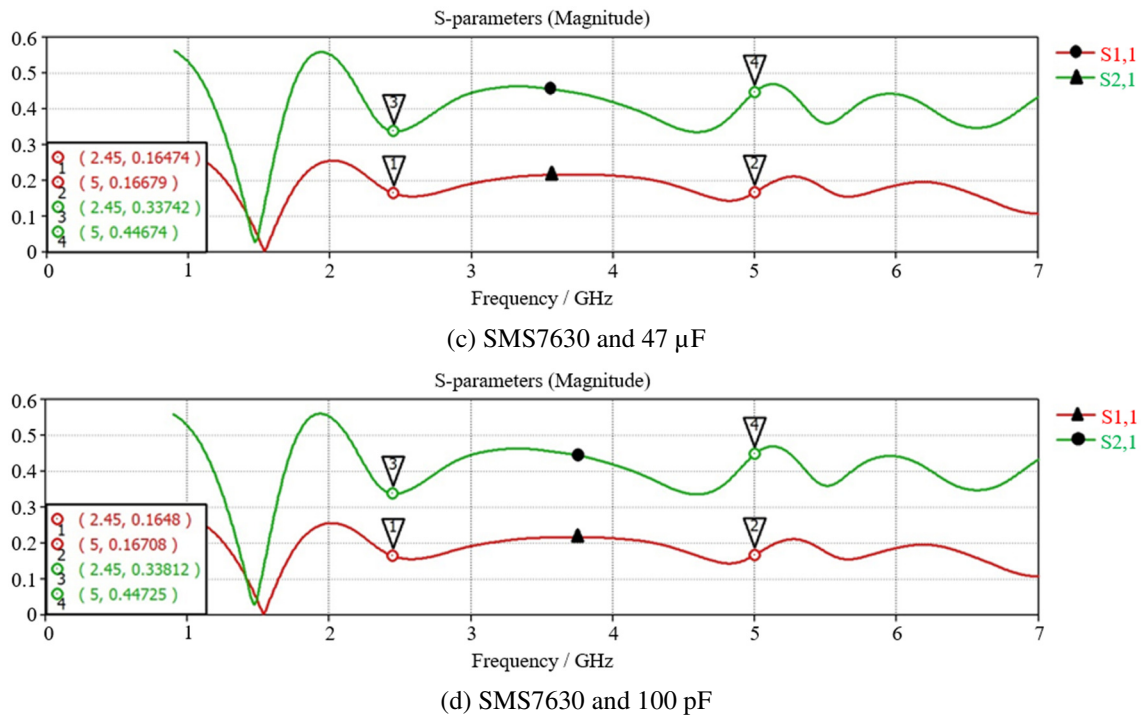


Fig. 22 The reflection and transfer coefficient (continued)

The details of the S-parameter results are tabulated in Table 6. As can be observed, the results indicate that all parameters are in good agreement, whether using SMS7630 or HSMS2852, with both capacitance values of 47 μF and 100 pF. Therefore, it can be proved that the proposed design of the CPW antenna with a rectangular patch is sufficient to integrate with the rectifier circuit for further use in RF energy applications.

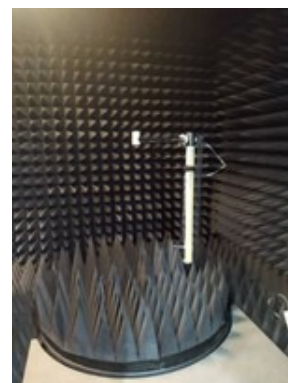
Table 6 S-parameter results of the integrated voltage doubler rectifier circuit and antenna design

Schottky diodes	Parameters	Frequency (GHz)	Reflection coefficient, S_{11}		Transfer coefficient, S_{21}	
			Magnitude	dB	Magnitude	dB
HSMS2852	C = 47 μF	2.45	0.16906	-15.439	0.16906	-15.439
		5	0.1571	-16.076	0.1571	-16.076
	C = 100 pF	2.45	0.1691	-15.437	0.1691	-15.437
		5	0.15745	-16.057	0.15745	-16.057
SMS7630	C = 47 μF	2.45	0.16474	-15.664	0.16474	-15.664
		5	0.16679	-15.557	0.16679	-15.557
	C = 100 pF	2.45	0.1648	-15.661	0.1648	-15.661
		5	0.16708	-15.542	0.16708	-15.542

5. Antenna Measurement



(a) Antenna performance measurement using the vector network analyzer



(b) Anechoic chamber for radiation pattern measurement

Fig. 23 Antenna measurement process

Upon the completion of the evolutionary antenna design and parameter optimization, the proposed CPW antenna with a rectangular slot patch was fabricated. To demonstrate the validity of this design, an experiment was devised that involved a vector network analyzer (VNA) and an anechoic chamber, as shown in Fig. 23. The VNA was used to evaluate one of the performance parameters, the reflection coefficient, of the developed patch antenna. Fig. 23(a) depicts the measurement process for the designed rectangular patch antenna, where the antenna was connected to the other end of the cable connected to the VNA. In this work, the radiation pattern performance of the developed rectangular patch antenna was measured utilizing an anechoic chamber model of the ATENLAB OTA-500, which can measure antenna performance from 600 MHz to 18 GHz. Fig. 23(b) depicts the antenna mounted on a stand embedded in a turntable on the receiver side.

Fig. 24 illustrates the plot of measured S-parameters compared with the simulated return loss of the proposed CPW antenna with a rectangular slot patch. The result exhibits good agreement between the measured and simulated reflection coefficients, S_{11} , for the 2.45 GHz and 5 GHz frequency bands, which are -15.2 dB and -13.8 dB, respectively. The 10 dB return loss bandwidths of simulation and measurement are from 2.15 GHz to 6.34 GHz and 2.16 GHz to 6.32 GHz, respectively. This indicates that the simulated and measured bandwidths are 4.19 GHz and 4.16 GHz, respectively.

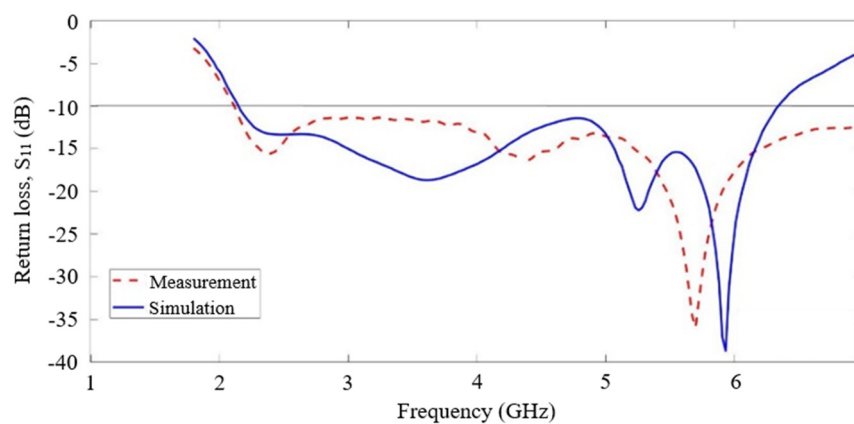


Fig. 24 Simulated and measured reflection coefficient of the proposed harvester antenna

The performance of the proposed work and comparison with the state-of-the-art are summarized in Table 7. The proposed antenna harvester can operate in a wide frequency range compared to other works. In Quddious et al. [20] and Dardeer et al. [21], the radiation efficiency for the 5 GHz frequency band is higher than in Srinivasu et al. [22], and this proposed work. However, the substrate used is considerably more expensive than FR-4. Even though the work of Dardeer et al. [21] achieves good performance in terms of radiation efficiency, the antenna design does not operate in UWB frequency, and the antenna size is also larger than this proposed work. Furthermore, Dardeer et al. [21] used Rogers RT6002, which results in a larger antenna dimension in terms of electrical wavelength. However, this does not contribute to gain improvement when compared to the results of this work. Zeya and Badhai [23] used the largest substrate and antenna size. Nevertheless, this approach did not enhance the antenna's gain as well as bandwidth.

Table 7 Circuit components specifications

Ref.	Substrate and antenna size (mm)	Antenna dimension (electrical wavelength)	Operating frequency band (GHz)	Antenna gain (dBi)	Radiation efficiency
[20]	Rogers RT/duroid 33 × 27 × 0.787	0.043	5-6.1	2.4 GHz:3	5.6 GHz:98%
[21]	Rogers RT6002 47 × 46.75 × 0.76	0.079	1.83-3.58	2.45 GHz:2.43	2.45 GHz:98.9%
			5.4-6	5.8 GHz:4.22	5.8 GHz:99.67%
[22]	FR-4 41 × 30 × 1.6	0.026	1.76-12.23	5 GHz:3.8	5 GHz:92 %
[23]	FR-4 50 × 50 × 1.6	0.072	2.1-3.0	2.4 GHz:3	NA
This work	FR-4 37 × 29 × 1.6	0.045	2.1-6.3	2.45 GHz:3.653	2.45 GHz:72%
				5 GHz:4.635	5 GHz:68%

6. Conclusions

In this research work, the proposed rectangular slot CPW UWB antenna is designed for ambient RF energy harvesting. The parametric analysis with the evolutionary design process has been performed for the proposed antenna, which aims to cover the Wi-Fi frequency bands of 2.45 GHz and 5 GHz and work as a harvester antenna. The antenna achieves UWB frequency ranges of 2.16 GHz to 6.32 GHz with an operating bandwidth of 4.16 GHz, which covers the UWB FBW of 105%. The findings indicate that the proposed CPW antenna with a rectangular slot is appropriate as a harvester antenna for Wi-Fi RF energy harvesting applications as it can capture ambient RF radiation covering a wide frequency range. The proposed CPW antenna with a rectangular slot is integrated with the voltage doubler rectifier circuit, and the performance is examined in terms of S-parameters. The findings from the S-parameters clarify that the proposed antenna significantly matched the doubler circuit. Thus, it can be concluded that the proposed antenna design can act as an antenna harvester for RF energy harvesting applications.

Conflicts of Interest

The authors declare no conflict of interest.

References

- [1] R. Kumar, Y. Kamatham, S. Peddakrishna, and A. Gaddam, "CPW-Fed Penta Band Monopole Antenna for Multiservice Wireless Applications," *Advances in Technology Innovation*, vol. 7, no. 1, pp. 66-76, January 2022.
- [2] R. S. Uqaili, J. A. Uqaili, S. Zahra, F. B. Soomro, and A. Akbar, "A Study on Dual-Band Microstrip Rectangular Patch Antenna for Wi-Fi," *Proceedings of Engineering and Technology Innovation*, vol. 16, pp. 01-12, August 2020.
- [3] S. M. Noghabaei, R. L. Radin, and M. Sawan, "Efficient Dual-Band Ultra-Low-Power RF Energy Harvesting Front-End for Wearable Devices," *IEEE 61st International Midwest Symposium on Circuits and Systems*, pp. 444-447, August 2018.
- [4] V. Palazzi, J. Hester, J. Bito, F. Alimenti, C. Kalialakis, A. Collado, et al., "A Novel Ultra-Lightweight Multiband Rectenna on Paper for RF Energy Harvesting in the Next Generation LTE Bands," *IEEE Transactions on Microwave Theory and Techniques*, vol. 66, no. 1, pp. 366-379, January 2018.
- [5] U. Muncuk, K. Alemdar, J. D. Sarode, and K. R. Chowdhury, "Multiband Ambient RF Energy Harvesting Circuit Design for Enabling Batteryless Sensors and IoT," *IEEE Internet of Things Journal*, vol. 5, no. 4, pp. 2700-2714, August 2018.
- [6] C. H. Lin, C. W. Chiu, and J. Y. Gong, "A Wearable Rectenna to Harvest Low-Power RF Energy for Wireless Healthcare Applications," *11th International Congress on Image and Signal Processing, BioMedical Engineering and Informatics*, pp. 1-5, October 2018.
- [7] Q. M. Dinh and M. T. Le, "Ambient RF Energy Harvesting System Based on Wide Angle Metamaterial Absorber for Battery-Less Wireless Sensors," *International Conference on Advanced Technologies for Communications*, pp. 140-144, October 2020.
- [8] H. Sun and W. Geyi, "A New Rectenna with All-Polarization-Receiving Capability for Wireless Power Transmission," *IEEE Antennas and Wireless Propagation Letters*, vol. 15, pp. 814-817, 2016.
- [9] C. Hannachi, S. Boumaiza, and S. O. Tatu, "A Highly Sensitive Broadband Rectenna for Low Power Millimeter-Wave Energy Harvesting Applications," *IEEE Wireless Power Transfer Conference*, pp. 1-4, June 2018.
- [10] D. K. Ho, V. D. Ngo, I. Kharrat, T. P. Vuong, Q. C. Nguyen, and M. T. Le, "A Novel Dual-Band Rectenna for Ambient RF Energy Harvesting at GSM 900 MHz and 1800 MHz," *Advances in Science, Technology and Engineering Systems Journal*, vol. 2, no. 3, pp. 612-616, 2017.
- [11] G. Srinivasu, N. Anveshkumar, and V. K. Sharma, "A Compact Octagon Slotted Circular UWB Antenna for RF Energy Harvesting," *International Conference on Emerging Trends in Information Technology and Engineering*, pp. 1-5, February 2020.
- [12] A. Costanzo, D. Masotti, M. Fantuzzi, and M. Del Prete, "Co-Design Strategies for Energy-Efficient UWB and UHF Wireless Systems," *IEEE Transactions on Microwave Theory and Techniques*, vol. 65, no. 5, pp. 1852-1863, May 2017.

- [13] H. Brunner, M. Stocker, M. Schuh, M. Schuß, C. A. Boano, and K. Romer, "Understanding and Mitigating the Impact of Wi-Fi 6E Interference on Ultra-Wideband Communications and Ranging," 21st ACM/IEEE International Conference on Information Processing in Sensor Networks, pp. 92-104, May 2022.
- [14] G. Breed, "A Summary of FCC Rules for Ultra Wideband Communications," High Frequency Electronics, vol. 4, no. 1, pp. 42-44, January 2005.
- [15] Malaysian Communications and Multimedia Commission, SKMM SRSP-549, 2013.
- [16] S. Muhammad, A. Smida, M. I. Waly, N. K. Mallat, A. Iqbal, S. R. Khan, et al, "Design of Wideband Circular-Slot Antenna for Harvesting RF Energy," International Journal of Antennas and Propagation, vol. 2022, article no. 5964753, 2022.
- [17] L. Aguni, A. El Yassini, S. Chabaa, S. Ibnyaich, and A. Zeroual, "Design of a Symmetric CPW-Fed Patch Antenna for WLAN/WIMAX Applications Using ANN," Wireless Personal Communications, vol. 115, no. 1, pp. 439-456, November 2020.
- [18] H. Tafekirt, J. Pelegri-Sebastia, A. Bouajaj, and B. M. Reda, "A Sensitive Triple-Band Rectifier for Energy Harvesting Applications," IEEE Access, vol. 8, pp. 73659-73664, 2020.
- [19] T. Sathiyapriya, V. Gurunathan, T. Vimala, K. N. K. Prasad, and T. N. Kumar, "Voltage Doubler Design for RF Energy Harvesting System," 7th International Conference on Smart Structures and Systems, pp. 1-4, July 2020.
- [20] A. Quddious, M. A. B. Abbasi, M. A. Antoniadis, P. Vryonides, V. Fusco, and S. Nikolaou, "Dynamically Reconfigurable UWB Antenna Using an FET Switch Powered by Wireless RF Harvested Energy," IEEE Transactions on Antennas and Propagation, vol. 68, no. 8, pp. 5872-5881, August 2020.
- [21] O. M. A. Dardeer, H. A. Elsadek, and E. A. Abdallah, "Compact Broadband Rectenna for Harvesting RF Energy in WLAN and WiMAX Applications," International Conference on Innovative Trends in Computer Engineering, pp. 292-296, February 2019.
- [22] G. Srinivasu, N. Anveshkumar, and V. K. Sharma, "A Circular Slotted Planar Monopole UWB Antenna for RF Energy Harvesting Applications," International Conference on Emerging Trends in Information Technology and Engineering, pp. 1-5, February 2020.
- [23] Z. Zeya and R. K. Badhai, "RF Energy Harvesting: Design of Printed Hexagon Antenna for ISM Band 2.4 GHz," 10th International Conference on Internet of Everything, Microwave Engineering, Communication and Networks, pp. 01-05, December 2021.



Copyright© by the authors. Licensee TAETI, Taiwan. This article is an open-access article distributed under the terms and conditions of the Creative Commons Attribution (CC BY-NC) license (<https://creativecommons.org/licenses/by-nc/4.0/>).